

## Structure and Mechanism of the Photoactivatable Green Fluorescent Protein

J. Nathan Henderson,<sup>†</sup> Rinat Gepshtein,<sup>‡</sup> Josef R. Heenan,<sup>†</sup> Karen Kallio,<sup>†</sup> Dan Huppert,<sup>‡</sup> and S. James Remington<sup>\*,†</sup>

*Institute of Molecular Biology and Department of Physics, University of Oregon, Eugene, Oregon 97403-1229, and Raymond and Beverly Sackler Faculty of Exact Sciences, School of Chemistry, Tel Aviv University, Tel Aviv 69978, Israel*

Received November 11, 2008; E-mail: jreming@uoregon.edu

The photoactivatable mutant PA-GFP, resulting from the single substitution threonine 203 to histidine (T203H), has become a popular optical label for real-time *in vivo* tracking experiments.<sup>1,2</sup> Upon UV activation, PA-GFP irreversibly switches from a form that is dark under 488 nm illumination to a brightly emissive form. One advantage of PA-GFP is the excellent contrast enhancement (~100-fold) following activation.<sup>1</sup> Here, we report X-ray crystallographic structures of native and activated PA-GFP along with the results of time-resolved fluorescence spectroscopy. Photoactivation is explained by a change in chromophore protonation state, resulting from the combined effects of the T203H substitution and photochemical degradation of Glu222. Furthermore, photoactivation of PA-GFP is mechanistically identical to the process previously described in the parent, wild-type GFP (WT).<sup>3</sup>

WT has two absorbance bands at 397 nm (A-band) and 475 nm (B-band) arising from equilibrium between the neutral and anionic chromophore forms, respectively. Excitation of either form gives rise to green fluorescence peaking at ~508 nm. In PA-GFP, the equilibrium in chromophore protonation is shifted toward the neutral form, strongly favoring A-band excitation (Figure 1). In addition, both the B-band absorbance and emission maxima are significantly red-shifted, to 505 and 515 nm, respectively.

In WT and PA-GFP, A band excitation produces the excited state (A\*), which then radiatively decays either through emission of a blue photon or via excited-state proton transfer (ESPT),<sup>4</sup> to generate an intermediate anionic excited state (I\*) that later emits a green photon (Figure S1). ESPT is typically more efficient than blue emission; hence the steady-state emission is green. In WT, photoactivation is an inefficient process that irreversibly converts form A into form B by photochemical decarboxylation of Glu222.<sup>3,5</sup> Rate measurements for photoactivation in WT and PA-GFP reveal similar kinetics in both proteins (Table S1).

To investigate the photoactivation process, we introduced the mutation T203H into the triple GFP mutant F99S/M153T/V163A<sup>3</sup> to create a “folding optimized” form of PA-GFP. These proteins display steady-state and time-resolved spectroscopic properties (Figures S2 and S3) that are indistinguishable from WT and PA-GFP; henceforth, the mutant F99S/M153T/V163A/T203H is referred to simply as PA-GFP. Isomorphous crystals of native and photoactivated PA-GFP grew in space group *P*2<sub>1</sub>2<sub>1</sub>2<sub>1</sub> with four monomers in the asymmetric unit. Data collection and atomic model refinement statistics are excellent (Table S2). With either PA-GFP structure, superposition of  $\alpha$ -carbons onto WT yields rms deviations of <0.50 Å for each of the four monomers in the asymmetric unit; however significant structural changes are observed adjacent to the chromophore.

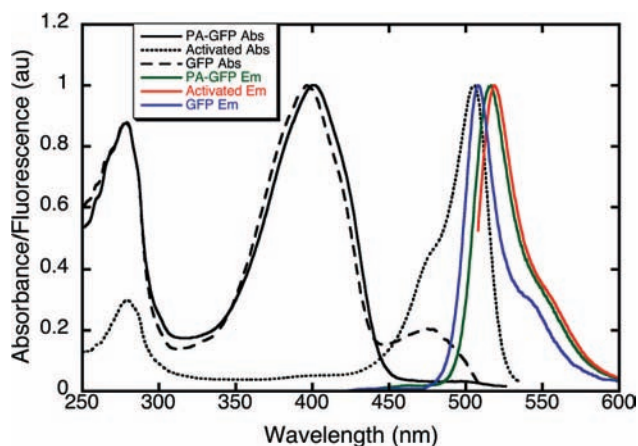


**Figure 1.** Absorption (Abs) and fluorescence emission (Em) spectra of native PA-GFP, photoactivated PA-GFP, and wild-type GFP (WT).

Comparison of the final  $2F_o - F_c$  electron density maps of native and photoactivated PA-GFP strongly suggests UV-induced decarboxylation of Glu222 (Figures 2A,B and S4). Previous studies of photoactivation in WT<sup>3,5</sup> demonstrated the same result, proposed to occur via a Kolbe mechanism. In both photoactivated PA-GFP and WT, the C $\gamma$ -methyl group of the remnant of Glu222 is pointed away from the chromophore. Two presumed water molecules occupy the space adjacent to the vacated carboxylate (Figures 2B and S4). Loss of electrostatic repulsion from Glu222 accounts for the shift in chromophore equilibrium toward the anionic B-state. Upon photoactivation of WT, Thr203 rotates toward the chromophore to form an additional hydrogen bond (three total) stabilizing the chromophore phenolate (Figure 2B). This interaction is not available in PA-GFP, and remarkably, the stacking interaction of His203 remains unaltered upon photoactivation (Figure 2A and B). In either charge state, the chromophore hydroxyl group forms two hydrogen bonds, one with His148 and one with an internal water molecule.

The structures also account for changes in excitation and emission spectra of PA-GFP relative to WT. The hydrogen bond deficit in activated PA-GFP is proposed to destabilize the negative charge density on the *p*-hydroxybenzylidene ring, in part accounting for the ~30 nm red shift in PA-GFP B-band absorbance (505 nm). This follows from theory,<sup>6</sup> which predicts charge transfer toward the chromophore imidazolinone moiety upon excitation of the anion. This result is in accord with conclusions from mutational studies on other fluorescent proteins.<sup>7</sup> Likewise, the His203-chromophore ring stacking may lower the energy of the excited state as suggested for the T203Y substitution of YFP.<sup>8</sup> We argue that His203 is neutral and remains so upon photoactivation. If instead it were protonated and charged, electrostatic interactions

<sup>†</sup> University of Oregon.

<sup>‡</sup> Tel Aviv University.

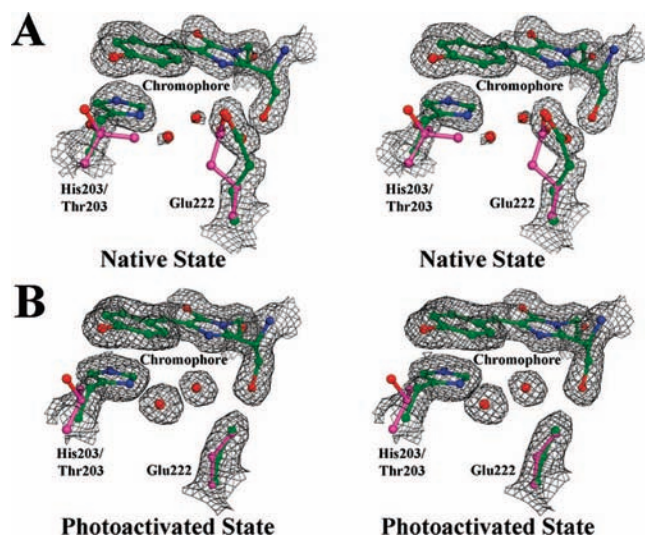


**Figure 2.** Stereoviews of the PA-GFP chromophore environment, showing  $1\sigma$   $2F_o - F_c$  electron density maps. (A) Comparison of Glu222 and residue 203 positions from native PA-GFP (green) and WT (magenta, PDB ID 1EMB). (B) Photoactivated PA-GFP (green) compared with photoactivated WT (magenta, PDB ID 1HCJ). Glu222 decarboxylation and ordering of water molecules are readily apparent. For several reasons (see Supporting Information), we interpret the apparent lower occupancy of the two water molecules in (A) to result from the disorder of Glu222, rather than partial photoactivation.

would oppose charge redistribution in the excited state and result in a blue shift, as observed with the cyan fluorescent protein amFP486.<sup>7</sup> Diminished charge redistribution has been proposed to account for the reduced Stokes shifts upon B-band excitation observed for several Thr203 variants.<sup>9</sup>

The T203H substitution affects the side chain conformation of Glu222, which is rotated away from His203 and occupies a slightly different position than that in WT. Nevertheless, the hydrogen bond network originally proposed<sup>10</sup> to promote proton transfer from the neutral chromophore to Glu222, through a bound water molecule and Ser205 in WT, remains intact (Figure S1). As evidence for ESPT in PA-GFP, deuterated samples display dramatically increased steady-state blue emission at the expense of green emission (Figure S5), suggesting reduced ESPT efficiency. Also, time-resolved emission measurements reveal large kinetic isotope effects for the decay of blue emission and rise of green emission (Figure S6). However, the time constant for proton transfer in PA-GFP is  $\sim 55$  ps at RT, which is  $\sim 3.5$  times slower than that observed for WT or the F99S/M153T/V163A variant, in accord with previous results<sup>9</sup> indicating reduced proton transfer efficiency in Thr203 variants.

Inspection of the PA-GFP model suggests two possible causes for the rate decrease in proton transfer. First, the orientation of the Glu222 carboxylate, the terminal proton acceptor,<sup>11</sup> may be geometrically less optimal for proton transfer than in WT. Second, the side chain appears to be partially disordered, as indicated by

vibrational parameters (B-factors) that are 50% higher than those of surrounding side chains. By comparison, the temperature factors of Glu222 in WT are on average only  $\sim 10\%$  higher than those of surrounding side chains. Recent studies using ultrafast IR spectroscopy and Density Functional Theory<sup>12</sup> suggest a relationship between the Glu222 side chain geometry and the proton transfer rate. These interpretations are consistent with a concerted ESPT model<sup>13</sup> where the orientation of the ultimate proton acceptor Glu222 limits the overall transfer rate.<sup>12–14</sup>

In PA-GFP, the large emission contrast between native and photoactivated states results from a dramatic change in the chromophore protonation state. The A state is favored by the T203H substitution, while the B state is favored by decarboxylation of Glu222. In principle, any substitution of Thr203 that favors the A state should be effective, possibly leading to new optical highlighters with different spectroscopic excitation and emission maxima. For example, we show here that GFP T203V/S205V,<sup>13</sup> which initially fluoresces blue upon 400 nm excitation, rapidly switches to a green fluorescent form with continued irradiation (Figure S7).

**Acknowledgment.** This work was supported by grants from the National Science Foundation (MCB-0720420) to S.J.R. and the Binational US-Israeli Science Foundation for S.J.R. and D.H. The Advanced Light Source is supported by the U.S. Department of Energy under Contract No. DE-AC02-05CH11231.

**Supporting Information Available:** Materials and methods, crystallographic statistics, supporting figures, and time-resolved fluorescence spectra. This material is available free of charge via the Internet at <http://pubs.acs.org>.

## References

- (1) Patterson, G. H.; Lippincott-Schwartz, J. *Science* **2002**, *297*, 1873–1877.
- (2) Shaner, N. C.; Patterson, G. H.; Davidson, M. W. *J. Cell Sci.* **2007**, *120*, 4247–4260.
- (3) van Thor, J. J.; Gensch, T.; Hellingwerf, K. J.; Johnson, L. N. *Nat. Struct. Biol.* **2002**, *9*, 37–41.
- (4) Chattoraj, M.; King, B. A.; Bublitz, G. U.; Boxer, S. G. *Proc. Natl. Acad. Sci. U.S.A.* **1996**, *93*, 8362–8367.
- (5) Bell, A. F.; Stoner-Ma, D.; Wachter, R. M.; Tonge, P. J. *J. Am. Chem. Soc.* **2003**, *125*, 6919–6926.
- (6) Voityuk, A. A.; Michel-Beyerle, M. E.; Rösch, N. *Chem. Phys.* **1998**, *231*, 13–25.
- (7) Henderson, J. N.; Remington, S. J. *Proc. Natl. Acad. Sci. U.S.A.* **2005**, *102*, 12712–12717.
- (8) Wachter, R. M.; Elsliger, M. A.; Kallio, K.; Hanson, G. T.; Remington, S. J. *Structure* **1998**, *6*, 1267–1277.
- (9) Kummer, A. D.; Wiehler, J.; Rehder, H.; Kompa, C.; Steipe, B.; Michel-Beyerle, M. E. *J. Phys. Chem. B* **2000**, *104*, 4791–4798.
- (10) Brejc, K.; Sixma, T. K.; Kitts, P. A.; Kain, S. R.; Tsien, R. Y.; Ormö, M.; Remington, S. J. *Proc. Natl. Acad. Sci. U.S.A.* **1997**, *94*, 2306–2311.
- (11) Stoner-Ma, D.; Jaye, A. A.; Matousek, P.; Towrie, M.; Meech, S. R.; Tonge, P. J. *J. Am. Chem. Soc.* **2005**, *127*, 2864–2865.
- (12) van Thor, J. J.; Ronayne, K. L.; Towrie, M.; Sage, J. T. *Biophys. J.* **2008**, *95*, 1902–1912.
- (13) Shu, X.; Leiderman, P.; Gepshtein, R.; Smith, N. R.; Kallio, K.; Huppert, D.; Remington, S. J. *Protein Sci.* **2007**, *16*, 2703–2710.
- (14) Vendrell, O.; Gelabart, R.; Moreno, M.; Lluch, J. M. *J. Chem. Theory Comput.* **2008**, *4*, 1138–1150.

JA808851N